

# Controlled Multibatch Self-Assembly of Microdevices

Xiaorong Xiong, Yael Hanein, *Member, IEEE*, Jiandong Fang, Yanbing Wang, Weihua Wang, Daniel T. Schwartz, and Karl F. Böhringer, *Member, IEEE*

**Abstract**—A technique is described for assembly of multiple batches of micro components onto a single substrate. The substrate is prepared with hydrophobic alkanethiol-coated gold binding sites. To perform assembly, a hydrocarbon oil, which is applied to the substrate, wets exclusively the hydrophobic binding sites in water. Micro components are then added to the water, and assembled on the oil-wetted binding sites. Moreover, assembly can be controlled to take place on desired binding sites by using an electrochemical method to deactivate specific substrate binding sites. By repeatedly applying this technique, different batches of micro components can be sequentially assembled to a single substrate. As a post assembly procedure, electroplating is incorporated into the technique to establish electrical connections for assembled components. Important issues presented are: substrate fabrication techniques, electrochemical modulation by using a suitable alkanethiol (dodecanethiol), electroplating of tin and lead alloy and binding site design simulations. Finally, we demonstrate a two-batch assembly of silicon square parts, and establishing electrical connectivity for assembled surface-mount light emitting diodes (LEDs) by electroplating. [839]

**Index Terms**—Capillary force, electrochemical modulation, electroplating, hydrophobicity, interfacial energy, micro assembly, reductive desorption, self-assembled monolayer (SAM), self-assembly, surface tension.

## I. INTRODUCTION

**I**N THE past two decades, major developments in micro electro mechanical systems (MEMS) have been founded on exploiting micromachining techniques and tools traditionally used for the silicon integrated circuits (ICs) industry. Current research in MEMS explores beyond what the name claims, and innovative materials and fabrication techniques have been combined with traditional semiconductor processes to build a wide range of micro functional devices (sensing, actuating, computing, etc.). Integrated micro systems consisting of these functional components will find promising applications in areas

such as telecommunications, chemical analysis and biomedical instrumentation. One major challenge in accomplishing such complex micro systems is the integration of different micro components. Monolithic integration of such systems is often limited by poor compatibility between components' fabrication processes or materials. Micro assembly provides a solution to circumvent these difficulties, and it allows micro devices to be fabricated and tested independently before they are integrated. Recently a number of techniques have been developed to assemble micro components into complex systems. A thorough study and discussions of various micro assembly strategies were presented by Cohn [1]. Conventional "pick and place" serial assembly methods have been adopted in the micro domain by using miniaturized robots and tools for organizing parts. There are two major concerns about this technique: serial manipulation and the "sticking problem". When a large number of parts need to be assembled, the time for assembly will be limited by the number of manipulators. In addition, with parts smaller than a millimeter, the adhesive forces between manipulator surfaces and parts, primarily due to electrostatics, van der Waals force or surface tension, are significant compared to gravitational force [2]. Special manipulators and additional tools are required to overcome these difficulties [3]–[6].

In order to accomplish efficient micro assembly of a very large number of components, parallel assembly approaches have emerged, falling into two major categories: deterministic and stochastic. In the deterministic class, assembly can be achieved by transferring microstructures between aligned wafers [7], [8]. In the stochastic category, assembly of a large number of identical micro parts occurs on specifically designed identical target sites. The assembly for all the micro components takes place simultaneously and the final assignment of each part to its destined site is random. We also use the term "self-assembly" to describe the stochastic assembly approaches, owing to the property that the assembly takes place in a spontaneous manner with components of specific design [9]. Various driving forces have been employed for self-assembly. Yeh and Smith developed a process to assemble trapezoidal micro components into complementary holes in a substrate using fluidic flow and gravitation [10]. Böhringer *et al.* have proposed a micro assembly approach by employing electrostatic fields as the driving force, with the aid of ultrasonic vibration to overcome and eliminate friction and adhesion [11]. In [12], an electrostatic self-assembly approach is applied to selectively pattern charged  $10\ \mu\text{m}$  gold disks on a substrate. Surface tension, capable of driving different micro scale motions for various applications: high-resolution wet printing [13], [14]; a liquid-metal micromotor [15];

Manuscript received March 29, 2002; revised December 12, 2002. This work was supported in part by the NSF Career Award ECS9875367 to K. F. Böhringer and by donations from Agilent Technologies, Intel Corporation, Microsoft Research, Tanner Research, Inc., and Technic, Inc. The work of D. T. Schwartz was supported in part by an NSF Young Investigator Award CTS-9457097. The work of Y. Hanein was supported in part by an NSF CISE Postdoctoral Research Associateship EIA0072744. The work of X. Xiong was supported by a Ford Fellowship. Subject Editor K. D. Wise.

X. Xiong, Y. Hanein, J. Fang, Y. Wang and K. F. Böhringer are with the Department of Electrical Engineering University of Washington, Seattle, WA 98195-2500 USA (e-mail: xrxiong@u.washington.edu).

W. Wang and D. T. Schwartz are with the Department of Chemical Engineering University of Washington, Seattle, WA 98195-2500 USA.

Digital Object Identifier 10.1109/JMEMS.2003.809964

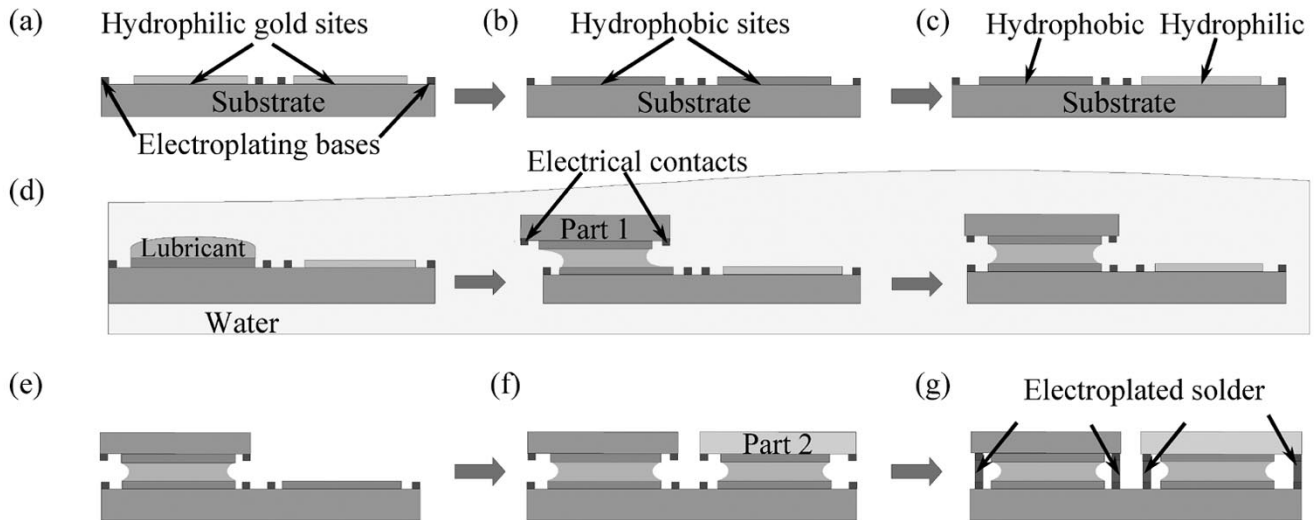


Fig. 1. Schematics of two-batch assembly steps: (a) A fabricated substrate with electrically isolated regions of hydrophilic Au binding sites and Ni electroplating bases. (b) Alkanethiol SAM adsorbed on Au patterns turns them hydrophobic. (c) Electrochemical SAM desorption from selected binding site (the right site) is used to de-activate it. (d) Application and partitioning of a hydrocarbon lubricant to a hydrophobic binding site, followed by assembly of the part and lubricant curing in an aqueous environment. (e) Deposition of alkanethiol SAM on the vacant Au binding site to activate it for another assembly. (f) Repeating the step in (d) for other micro parts. (g) Establishing electrical connections between assembled parts and the substrate by electroplating. Note that the vertical dimensions have been exaggerated for illustration purposes.

three-dimensional hinged micro structures [16], can also be involved as the driving force for micro assembly. Syms *et al.* reviewed the state of art surface-tension driven self-assembly approaches in [17]. Whitesides and coworkers first developed a strategy driven by capillary force to assemble simple electrical circuits [18], [19], and later three-dimensional electrical networks [20]. Srinivasan *et al.* adopted the capillary force driven assembly technique in [18], [19] to assemble microscopic parts onto desired sites on silicon and quartz substrates [21], [22]. In this technique, the substrate had hydrophobic alkanethiol SAM-coated gold patterns on hydrophilic background. A hydrocarbon lubricant, deposited exclusively on the hydrophobic patterns, attracted and assembled the microscopic parts in water, and it was then cured to physically bond the parts. Recently, self-assembly arrays of GaAs/GaAlAs LEDs on a flexible curved substrate was demonstrated in [23]. In this approach, metal solder was used as the lubricant to establish both physical and electrical connectivity between the LEDs and a flexible substrate. In all the studies in [18]–[23] parallel assembly was performed with identical components in a single batch. However, in most micro systems, integration of multiple devices is desired.

In the area of cell biology, patterning of different cell populations has been successfully demonstrated [24]. To attach each type of cell cultures onto a substrate, different regions were activated by electrochemically changing the surface chemistry. This method used specific chemistries to attach cells, and cannot be applied to generic assembly.

For general micro devices assembly, we develop a new approach to assemble multiple batches of components. In our approach, assembly is driven by capillary force and it proceeds on specially treated hydrophobic sites on the substrate. With the ability to change the surface chemistry, we are able to selectively assemble different batches of components on a single substrate.

Electrochemical modulation of the hydrophobicity of specific binding sites is used to alter the driving force for assembly. With this innovation, assembly can be controlled to take place only on desired binding sites. By repeating the process to activate different sites on the substrate for assembly, different batches of micro parts can be assembled on a single substrate in a sequential manner. Electroplating is exploited as a post assembly process to establish electrical connections for assembled components, such as LEDs.

In the following sections, we discuss important issues of the technique: principal concepts of our two-batch micro assembly process, experimental details of the processes, and a simulation tool to evaluate and choose assembly binding site design for the substrate.

## II. PROCESS CONCEPT

In Fig.1(a)–(g), we illustrate the schematic flow of our self-assembly approach, which is explained step by step in this section. First, a supporting structure destined for the assembly (referred to as “substrate” hereafter) is fabricated with exposed clean hydrophilic gold (Au) patterns [see Fig. 1(a)]. The assembly “parts”, defined as those objects that are to be assembled, are prepared with corresponding patterns. For simplicity, we use the term “binding sites” for the exposed gold patterns on the substrate and the corresponding patterns on the parts.

Second, the substrate is soaked in ethanolic alkanethiol ( $CH_3(CH_2)_nSH$ ) solution and a hydrophobic alkanethiol self-assembled monolayer is chemisorbed on the exposed Au patterns [25]. The SAM adsorption activates all the Au binding sites on the substrate for assembly. The remaining areas on the substrate stay hydrophilic [see Fig. 1(b)]. In order to control the assembly to take place on selected

binding sites, we use an electrochemical method to modulate the hydrophobicity of the binding sites we wish to deactivate [see Fig. 1(c)]. Electrochemical desorption of alkanethiol SAM from these binding sites [26], [27], i.e.,  $CH_3(CH_2)_nSAu + e^- \rightarrow Au + CH_3(CH_2)_nS^-$  changes them from hydrophobic to hydrophilic. Based on reductive desorption characterization of different alkanethiol SAMs, discussed later in the text, we chose dodecanethiol ( $CH_3(CH_2)_{11}SH$ ) for our assembly experiments. After the desorption process, assembly occurs only at the hydrophobic binding sites.

Fig. 1(d) depicts the assembly process, which includes lubricant application, part transferring and alignment steps. For assembly, the capillary driving force is created by a hydrocarbon-based lubricant liquid bridge between binding sites on a part and on a substrate in an aqueous environment. The lubricant is spread on the dry substrate. Since the interfacial tension of the lubricant-SAM interface ( $\gamma < 1 \text{ mJ/m}^2$  [28]) is much lower than the interfacial tension of the water-SAM interface ( $\gamma \approx 50 \text{ mJ/m}^2$  [28]), the lubricant wets only the SAM-coated hydrophobic patterns after being immersed in water. Parts are then transferred into water. The capillarity aligns the part to a binding site on the substrate. This self-alignment phenomenon is the result of minimization of the interfacial energy between the lubricant bridges and water. Next, the lubricant is polymerized by heat and the parts are permanently bonded to the substrate. During the assembly process, the hydrophilic Au binding sites which have gone through SAM desorption remain clean and are reserved for future assembly. By repeating the SAM adsorption and assembly process, another batch of micro parts can be assembled on the vacant binding sites [see Fig. 1(e) and (f)].

After assembly, different micro parts are physically bonded to the substrate. In most cases, electrical connections and controls for these parts are needed. An electroplating method has been investigated for this purpose. By electroplating, metal alloy can be deposited on the plating bases on the substrate to establish electrical connections between the assembled parts and the substrate in a parallel manner [see Fig. 1(g)].

We have so far discussed the principles of our technique. We now turn to describe the fabrication and experimental details for our multibatch micro assembly process.

### III. EXPERIMENTAL APPROACHES

In this section, we describe the principal experimental methods used to perform the self-assembly. This includes the fabrication process of suitable substrates and parts, SAM adsorption and selective desorption, assembly setup, and finally, the electroplating process.

#### A. Fabrication of Substrates and Parts

1) *Test Part Fabrication:* For two-batch assembly, we use two types of  $1 \times 1 \text{ mm}$  silicon test parts. The first batch parts have square Au patterns ( $1 \times 1 \text{ mm}$ ) on one side, serving as the binding site, and Au patterns of  $0.8 \times 0.8 \text{ mm}$  on the other side. The second batch parts are patterned with  $1 \times 1 \text{ mm}$  Au binding sites on one side. The second batch of parts are fabricated by dicing a silicon wafer, which has an adhesion layer of

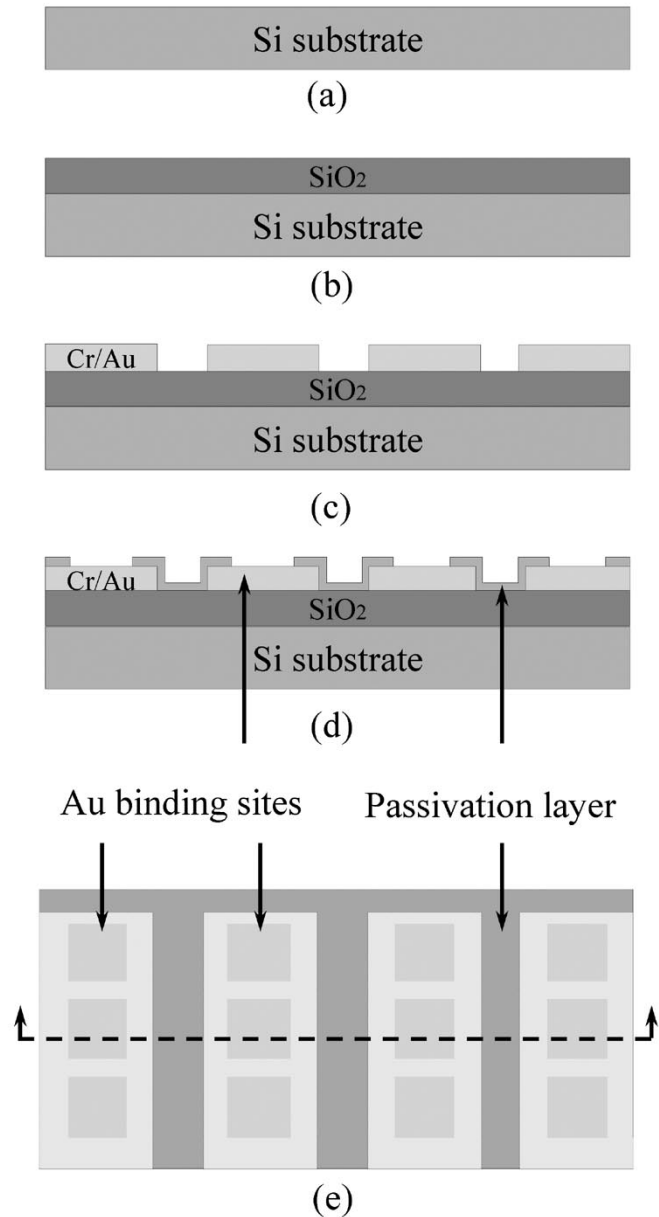


Fig. 2. Fabrication flow of substrates designed for square test parts assembly. (a) Silicon substrate. (b) Silicon dioxide layer, which isolates the silicon substrate from the metal layer. (c) Cr–Au metallization layer. Here, this layer is patterned as an array of electrically isolated stripes. (d) Passivation layer of SOG. This layer has openings that expose the square binding sites on the Au stripes. (e) Top view of a fabricated substrate.

$100 \text{ \AA}$  chrome (Cr) and  $1000 \text{ \AA}$  Au sputtered on the polished side. The square test parts are used as fabricated without any further process. Untreated Au surfaces have a contact angle of  $70^\circ$  [29] after exposure to lab atmosphere, which is sufficient to ensure assembly.

Commercial devices, i.e., surface mount LEDs ( $0.8 \times 1.6 \text{ mm}$ , Lumex), are used as assembly components to demonstrate the electroplating method.

2) *Substrate Fabrication:* In Fig. 2(a)–(e), we show the schematic fabrication flow of a substrate designed to support self-assembly of square test parts. The substrate is prepared with a thermal oxidation layer of approximately  $4500 \text{ \AA}$  as an isolation layer on a  $3''$  (100) silicon wafer [see Fig. 2(b)].

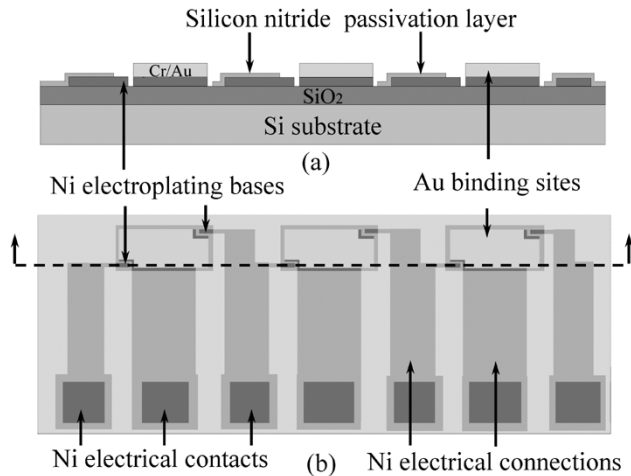


Fig. 3. Schematic plots of a fabricated substrate to support LED assembly and electroplating. (a) Cross-section of the substrate. (b) A top view of the substrate.

Next, a layer of Cr–Au is patterned on the substrate by a lift-off process. The substrate is first patterned with photoresist (AZ1512, Clariant), followed by sputtering of Cr (100 Å) and Au (1000 Å) on the substrate. The photoresist is then dissolved by acetone, and the metal layer is patterned on the substrate [see Fig. 2(c)]. The wafer is then cleaned with isopropyl alcohol (IPA), deionized (DI) water and dried with N<sub>2</sub>. An approximately 3000 Å passivation layer of spin-on glass (SOG) (311, Honeywell) is spun on and cured, before photoresist AZ1512 is patterned as a mask to define the SOG pattern. This step is followed by a reactive ion etch (RIE, Trion Technology) of CH<sub>3</sub>F with O<sub>2</sub> to expose the Au binding sites. Finally, the substrate is cleaned with acetone to strip off the photoresist, rinsed with IPA, DI water and dried with N<sub>2</sub> [see Fig. 2(d) and (e)].

Fig. 3(a) and (b) shows the cross section and a top view of a substrate designed for LED assembly and to demonstrate electroplating. To prepare such a substrate, a Cr–Au layer is patterned as the binding sites for assembly. Additional metallization layers of 100 Å Cr and 250 Å nickel (Ni) are thermally evaporated and patterned by lift-off, prior to the Cr/Au layer deposition. This additional Cr–Ni layer is patterned as electroplating metal bases for electroplating, as well as the connections between the Au binding sites and the electrical contacts [see Fig. 3(b)]. The electrical contacts serve as an interface to the external electrical control for the electroplating process, and to activate the LEDs afterwards. Silicon nitride (3000 Å) is sputtered as a passivation layer. The passivation layer is patterned photolithographically with an adhesion layer of primer (prime-P10, Shin-EtsuMicroSi) and AZ1512 photoresist. Finally, RIE of SF<sub>6</sub> is used to etch the nitride layer to expose the binding sites and the electroplating bases. This step is followed by acetone, IPA, and DI water cleaning and N<sub>2</sub> dry.

### B. Surface Cleaning

Due to the nonpolar contaminants adsorbed on the high free energy Au surface [29], a cleaning process is crucial for our experiments. We use two minutes of oxygen plasma to clean the substrate.

### C. SAM Adsorption

Immediately after the oxygen plasma treatment, the cleaned substrate is placed into a glass container with freshly prepared alkanethiol solution. The solution is prepared with 1 mM dodecanethiol (CH<sub>3</sub>(CH<sub>2</sub>)<sub>11</sub>SH, Aldrich) in ethanol, and the substrate is soaked in the solution for at least two hours to allow SAM adsorption. Thus, an alkanethiol monolayer is deposited on the exposed Au areas on the substrate. After the adsorption process, the exposed Au binding sites turn hydrophobic with a contact angle in the range of 110° [29].

### D. Gold on Mica Samples

For the purpose of characterizing different alkanethiol SAM desorptions, we use single crystalline Au(111) thin film, evaporated on mica [30]. The samples are soaked in 1 mM alkanethiol (CH<sub>3</sub>(CH<sub>2</sub>)<sub>n</sub>SH, n = 2, 7, 11, 17, Aldrich) solutions in ethanol for at least two hours to allow SAM adsorption.

### E. SAM Desorption

The electrochemical desorption of alkanethiol SAMs is employed to modulate surface hydrophobicity. Reductive desorption of SAMs is performed in a conventional three-electrode electrochemical cell [31]. SAM coated Au surfaces, i.e., the binding sites on fabricated wafers and Au(111) on mica samples, act as the working electrodes. The counter electrode is a platinum mesh. A saturated calomel electrode (SCE, Accumet) is used as the reference electrode. The electrolyte is 0.5 M (pH = 13.5) aqueous KOH (Fisher Scientific) solution. The potential is controlled between the working and the reference electrodes, and the current which passes through the working electrode, electrolyte and the counter electrode is measured. The control of the cell is performed by a potentiostat. Cyclic voltammetry (CV) (i.e., the repeated scanning of the working electrode potential) is performed to monitor and characterize the desorption of SAMs from working electrode surfaces [27]. The potential windows for the CVs are from 0 V to –1.4 V versus SCE. Lower pH solutions are not feasible, as the low desorption potentials of the SAMs (below –1 V versus SCE) would have strong interference from the co-evolution of H<sub>2</sub>.

### F. Assembly and Electroplating

After desorption of SAMs from the Au surfaces, the substrate is removed from the electrochemical bath, rinsed with DI water and dried with N<sub>2</sub>. A hydrocarbon lubricant is spread on the clean, dry substrate by a pipette. The substrate is slid manually and slowly into DI water in a petri dish until it is completely immersed in water. Lubricant forms droplets on the hydrophobic binding sites. Parts are then rinsed with DI water in a vial. Afterward, water with parts is poured into the petri-dish. With agitation, the assembly takes place exclusively on the hydrophobic areas with lubricant. The agitation is provided either by an orbital shaker or by manual shaking.

Here we use a heat-curable lubricant composed of 97 wt.% triethyleneglycol dimethacrylate (Sigma) as a monomer, and 3 wt.% benzoyl peroxide (Sigma) as the thermal initiator [32]. The lubricant, completely polymerized at 80 °C in water after

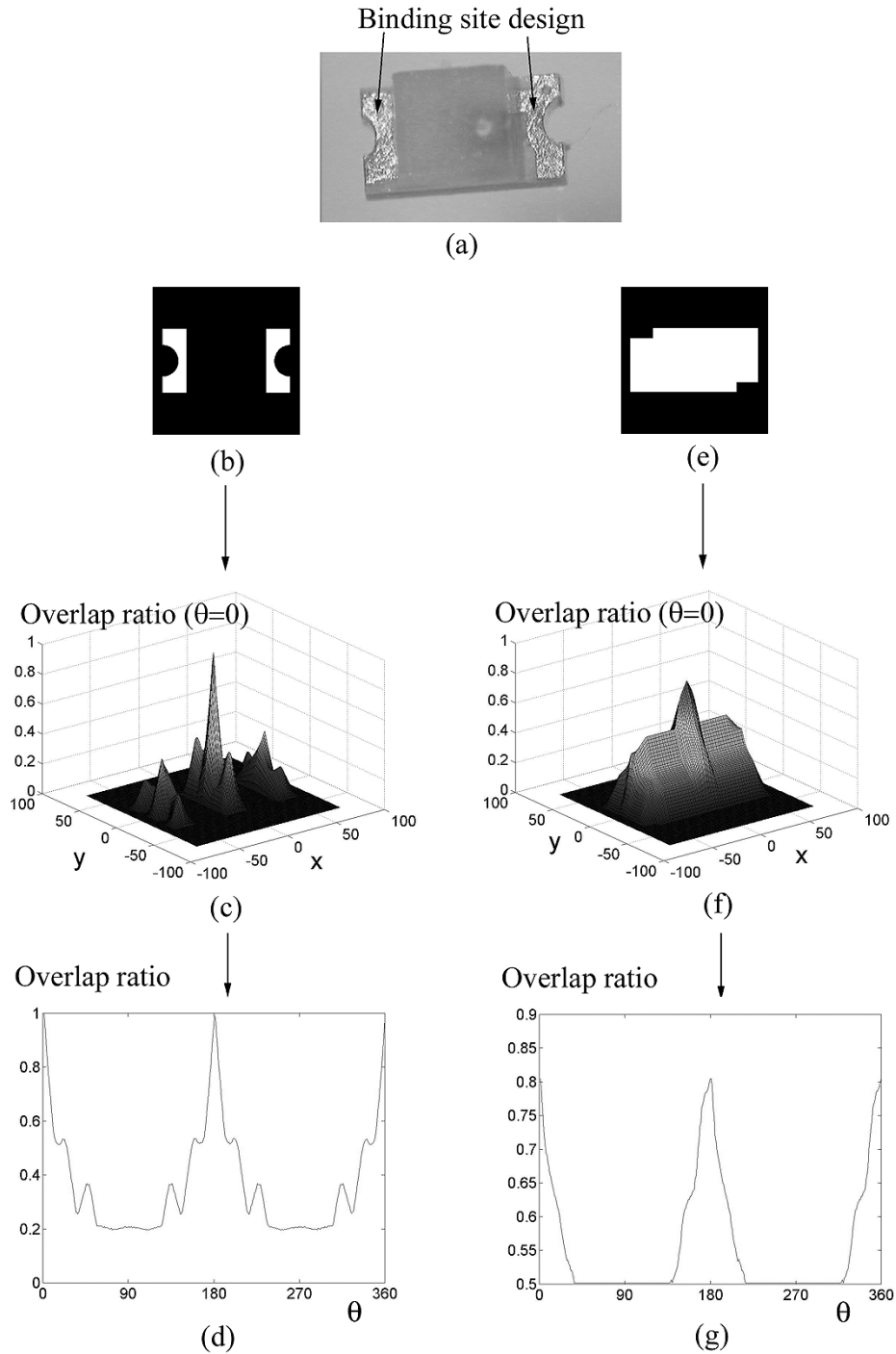


Fig. 4. (a) A commercial LED with the given binding site design. (b) An intuitive design for the substrate binding site is the same as the binding site pattern of the LED. (c) Translation and (d) rotation simulations for the design in (b). (e) Another binding pattern design for LED assembly, with the openings on the top-left and bottom-right corners for placing the electroplating bases. (f) Translation and (g) rotation simulations for the design shown in (e).

approximately an hour, permanently bonds the parts to the binding sites.

The plating process employs a platinum mesh as an anode and the plating bases on the substrate as a cathode. The bath is a commercial solder solution (Technic solder matte NF 820 HS (60/40), Technic Inc.). The plated solder is an alloy of lead (Pb) 40 wt.% and tin (Sn) 60 wt.%. The current density for plating is  $300 \text{ mA/cm}^2$ , and the plating rate is approximately  $5 \mu\text{m/min}$ . The resistivity of the alloy is approximately  $1.4 \times 10^{-7} \Omega\text{m}$ .

#### IV. BINDING SITE DESIGN

Binding site design is important for assembly, since optimal binding site design would allow high alignment accuracy, high assembly yield, short assembly time, and the uniqueness of assembly orientation. When using commercial off the shelf components such as LEDs with given design shown in Fig. 4(a), a straightforward design would simply use the same pattern as the part binding site shape. However, it is shown that such a de-

sign will not always be optimal and misalignment may occur in assembly [33]. To improve assembly, we custom design the binding site and plating basis geometry using a software simulation tool [33], [34].

The simulation tool is based on a simple surface energy model of our self-assembly system. It uses the observation that self-assembly and self-alignment is the result of minimization of interfacial energy between the lubricant meniscus and the aqueous environment. As described in [33], [34], the interfacial energy is directly proportional to the exposed hydrophobic surfaces in water. In [35], the simulation of the surface energy versus overlap area of a square shape binding site is carried out by a finite element software called *surface evolver* [36]. The result shows the surface energy is linear with the lateral displacement, when the displacement is beyond the range of the lubricant thickness. In a first-order approximation, the surface energy  $W$  can be represented in terms of the hydrophobic regions on the part and the substrate, denoted by  $P$  and  $S$  respectively, as long as the lubricant bridge height is small compared to the binding site length and width

$$W = \gamma (|S| + |P| - 2|S \cap P|). \quad (1)$$

Here  $\gamma$  is the interfacial energy coefficient, and  $|S|$  and  $|P|$  denote the surface area of region  $S$  and  $P$  respectively. Since the terms  $|S|$  and  $|P|$  in (1) are constants,  $W$  is directly proportional to  $-|S \cap P|$ : the negated overlap area between  $S$  and  $P$ .

To briefly describe the implementation of the simulation tool, the overlap area called  $A(x, y, \theta)$  is computed with respect to three parameters, representing the relative location  $(x, y)$  and orientation  $\theta$  of  $P$  to  $S$ . For a given orientation  $\theta$ , the value  $A$  can be calculated efficiently by two-dimensional convolution of  $P$  to  $S$ . To characterize the overlap area as a function of rotation angle, calculations are iterated for discretized  $\theta$  values in the range from  $0^\circ$  to  $360^\circ$ . Therefore, for a binding site design, we use two plots to show the simulation results: translation and rotation. In the translation result, the overlap ratio, which is the ratio of the overlap area to part binding site area ( $(|S \cap P|)/|P|$ ), is plotted as a function of relative location  $(x, y)$  of  $P$  to  $S$ . In the rotation result, each point in the plot corresponds to a maximum overlap ratio with respect to a given orientation  $\theta$ .

Ideally, assembly configurations should possess a unique global energy minimum, which, according to our model, would correspond to a unique maximum of area overlap as a function of  $(x, y, \theta)$ . With the given symmetric LED binding site design shown in Fig. 4(a), such a unique maximum is impossible to achieve. Fig. 4(b) and (e) shows two different binding site designs, and the design in Fig. 4(b) is simply the same as the LED binding site design. Fig. 4(c) and (d) shows the translation and rotation simulation results for design (b), and Fig. 4(f) and (g) shows the simulation results for design (e). Fig. 4(c) shows multiple local maxima for binding site design Fig. 4(b) at  $0^\circ$ , while Fig. 4(f) shows only one maximum for design Fig. 4(e). Fig. 4(d) and (g) shows that design (b) has multiple maxima at various orientations, while design (e) has only two maxima for  $0^\circ$  and  $180^\circ$  (there must be two maxima because the LED design is symmetric). These simulation results indicate that design (b) is preferable, as it exhibits only two maxima in overlap.

## V. RESULTS AND DISCUSSIONS

We have described the experimental details of our approach to incorporate two new methods into the micro assembly tool box: 1) selective desorption of SAM from patterned surfaces to allow multibatch assembly and 2) electroplating to establish electrical connectivity of assembled parts. To demonstrate these capabilities we fabricate and test substrates and parts specifically designed for these applications. Our results and related discussions are presented below.

### A. Selective Desorption

In our experiments, we use dodecanethiol ( $CH_3(CH_2)_{11}SH$ ), which is based on the considerations of monolayer stability and desorption time. Previous studies [25] show that monolayers formed by alkanethiols with longer chain lengths are more densely packed. This affects the stability and desorption time of the monolayer. To find an optimal alkanethiol forming stable SAM for assembly, but also possessing desorption time suitable for our application, we have explored reductive desorption of different alkanethiol SAMs ( $CH_3(CH_2)_nSH$ ,  $n = 2, 7, 11, 17$ ) respectively. Cyclic voltammograms, obtained from single crystalline Au(111) on mica [26], [27], have been used for characterization.

Fig. 5(a)–(c) shows results from the reductive desorption experiments of Au(111) on mica samples. The clear negative current peaks in the CVs indicate the reductive desorption of alkanethiol SAMs from the surfaces. These peaks become less pronounced with additional CV scanning cycles, implying the decreasing coverage of SAMs. The disappearance of the desorption peaks indicates that a major portion of the SAM has been desorbed. The desorption peak shifts systematically with carbon chain length, with the  $CH_3(CH_2)_7SH$ ,  $CH_3(CH_2)_{11}SH$  and  $CH_3(CH_2)_{17}SH$  peaks being at  $-1.05$  V,  $-1.2$  V and  $-1.35$  V versus SCE [see Fig. 5(a)–(c)]. Also, the time needed to desorb the SAMs varies systematically with chain length. For example, the longest alkanethiol SAM assessed,  $CH_3(CH_2)_{17}SH$ , still has a significant fraction on the surface after one hour and half of desorption [see Fig. 5(c)]. On the other hand, we observe that the surface with propanethiol SAM changes hydrophobicity in the KOH solution even in the absence of an applied potential. Therefore, propanethiol is ruled out as a choice for the assembly experiment. The longer desorption time for the longer chain length alkanethiol SAMs might be the result of readsorption of the reduced products. The discussions in [37] suggest that the readsorption is attributed to the solubilities and diffusion rates of the alkanethiol desorption products, with the longer alkanethiols having the lower solubility and diffusion rate.

By comparing desorption time [see Fig. 5(a)–(c)] and stability of the different alkanethiol SAMs, dodecanethiol ( $CH_3(CH_2)_{11}SH$ ) is chosen for the assembly experiments. The dodecanethiol forms stable hydrophobic SAM on Au, and desorption of a major fraction of the monolayer takes approximately 15 min implied by the disappearance of the desorption peak in the dotted CV data in Fig. 5(b).

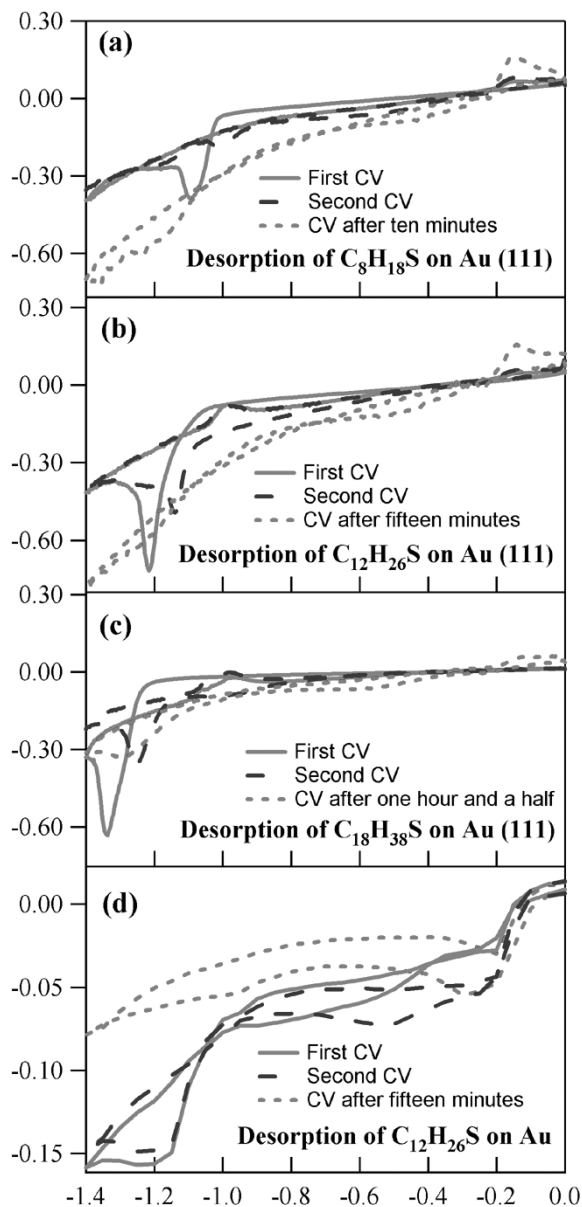


Fig. 5. (a)–(c) CVs of SAM desorption from Au(111) on mica. (a) Octanethiol ( $C_8H_{18}S$ ). (b) Dodecanethiol ( $C_{12}H_{26}S$ ). (c) Octadecanethiol ( $C_{18}H_{38}S$ ). (d) CVs of dodecanethiol ( $C_{12}H_{26}S$ ) SAM desorptions from polycrystalline Au on Si.

Desorption of dodecanethiol SAM from polycrystalline Au patterns on a Si substrate is shown in Fig. 5(d). These desorption CVs have broader peaks, compared with desorption CVs from single crystalline Au on mica. Moreover, it is observed that the time needed to desorb the SAM to turn the Au surface hydrophilic is longer than the time measured by the disappearance of the desorption peak. The average desorption time for the designs shown in Fig. 2(e) is around one hour for dodecanethiol SAM.

### B. Two Step Assembly and Yield

A substrate shown in Fig. 2 is used to demonstrate two step assembly of square test parts. The substrate is first coated with dodecanethiol SAM [see Fig. 1(b)]. Then potential bias is applied to selected electrically addressable sites in an electrochemical

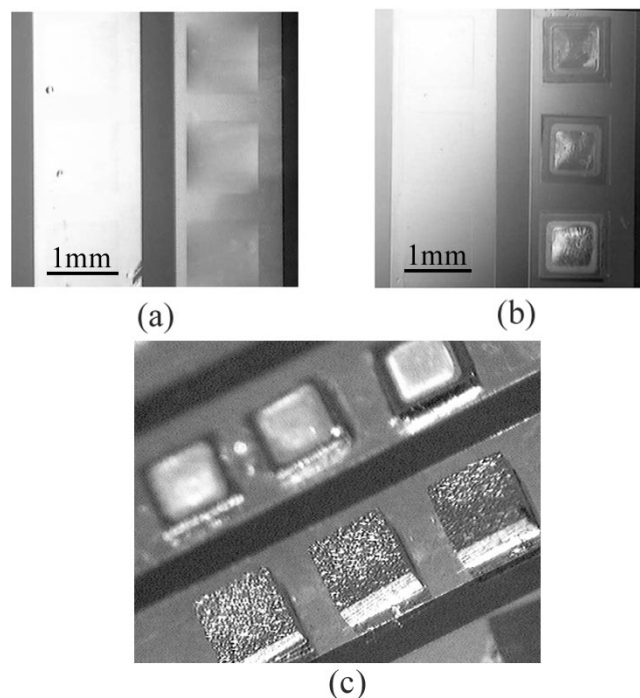


Fig. 6. (a) Substrate with lubricant in water after selective SAM desorption. Reductive desorption has removed the SAM from the Au squares on the left column. Lubricant wets the Au squares with SAM. (b) First batch of  $1 \times 1$  mm parts have been assembled and bonded only to Au patterns with lubricant on the right. (c) Side view of two-batch controlled micro assembly. Foreground: Second batch of  $1 \times 1$  mm assembled parts. Background: First batch of assembled parts.

cell, and these sites undergo electrochemical desorption to return them to the hydrophilic state [see Fig. 1(c)]. After SAM adsorption and one hour of selective desorption, the substrate with a thin layer of lubricant is immersed in water [see Fig. 1(d) without part]. The different lubricant wetting properties of Au binding sites with and without SAM are readily seen in Fig. 6(a). The Au squares without SAM on the substrate remain lubricant free [see Fig. 6(a)]. Next, a first batch of parts are added to the aqueous phase and assembled on the lubricant coated binding sites [see Fig. 6(b)]. After curing the lubricant, cleaning the substrate with acetone, IPA and DI water and drying it with  $N_2$ , a second assembly is performed by repeating steps described in Fig. 1(e) and (f). An example of two-batch assembly is shown in Fig. 6(c). By repeating SAM adsorption, desorption and assembly, controlled micro assembly is feasible, in principle, for a large number of batches.

In the assembly experiments, one must select criterion (e.g., yield) for successful assembly. The simplest criterion is the fraction of binding sites that have assembled parts on them. For the assembly of the square parts, we use this criterion to determine the yield. In a simple yield test with square parts, 14 out of a four by four array had assembled components. The assembly occurred within two minutes. The failures were mostly due to the agitation of the assembly. For example, flipped parts usually are not assembled, if agitation of the parts is two-dimensional and provided by an orbital shaker. In addition, the capillary driving force starts to work only when the part has contact with the lubricant. The binding sites would remain unoccupied, if there are no parts that come into contact with it. An improved setup is

TABLE I  
COMPARISONS BETWEEN ELECTROPLATING BASIS MATERIALS

Metals	Process compatibility	Adhesion with alloy
Au	compatible.	good
Al	compatible.	poor
TiW	incompatible	poor
Ni	compatible.	good

used which allows manual shaking for three-dimensional parts agitation. Furthermore, providing excess parts into the system can improve the yield. In [23], two cycles of assembly and re-collecting incorrectly assembled parts were repeated to achieve better yield.

Our multi-batch assembly approach can be applied to a range of different micro parts. These parts have to be compatible with all assembly processes, such as electrochemical desorption, lubricant curing and electroplating.

Furthermore, with assembled micro parts having hydrophobic patterns on the backside, the repeatability of the assembly process might be limited. In such a situation, the lubricant will wet the hydrophobic patterns on the assembled components, and parts from the next batch will be attracted to these patterns during the later assembly step. On the other hand, this could be useful, if three dimensional stacks of parts are desired.

### C. Electroplating Basis Material

We now turn to demonstrate the use of an electroplating method to establish electrical connections to the assembled parts. Our choice of the electroplating basis metal is mainly based on the following considerations: compatibility with the substrate fabrication process and adhesion with electroplated alloy. Different metals: Au, aluminum (Al), titanium-tungsten (TiW) and Ni have been tested. The results are summarized in Table I.

TiW is incompatible with the oxygen plasma cleaning process, as it is etched during the process. The poor adhesion on Al and TiW is due to their native oxide layer, while Au does not have such a native oxide layer. As a result, the plated alloy has uneven profile on Al and TiW plating bases. Good adhesion between Ni plating basis and the plated alloy is observed, despite the Ni oxide layer, which is thinner than the Al oxide [38]. The thin Ni oxide can be reduced at the plating potential in the acid electroplating solution, thus allowing good adhesion.

To demonstrate the electroplating method, we use LEDs for assembly by repeating the process described in Fig. 1(a)–(d). The results are shown in Fig. 7. In Fig. 7(a), we show a Au binding site with two Ni plating bases. The design is chosen based on the simulation results in Fig. 4. No alkanethiol SAM is formed on the oxide coated Ni during the adsorption process. Thus during the assembly process, the lubricant does not wet the Ni plating bases, leaving them clean for electroplating [see

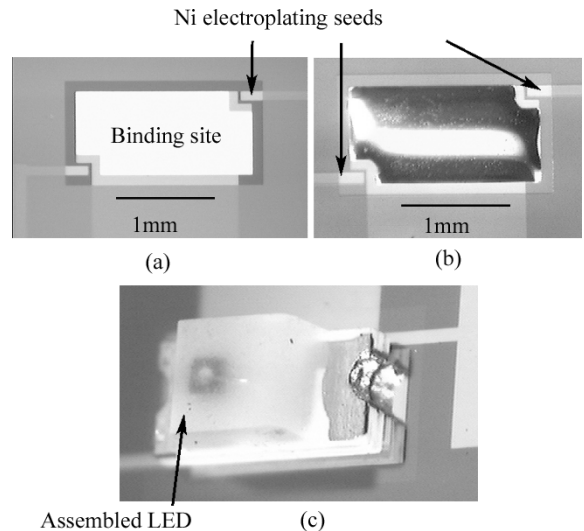


Fig. 7. (a) Binding site designed for LED assembly. (b) Binding site with SAM after lubricant is applied. The exposed Ni electroplating bases remain clean. (c) Assembled LED on a binding site.

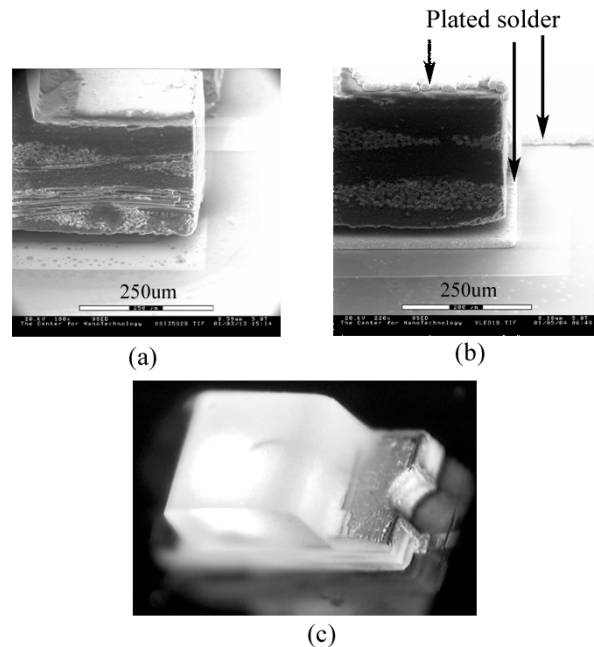


Fig. 8. (a) ESEM image of an assembled LED. (b) ESEM image of an assembled LED after electroplating. (c) LED on a substrate after electroplating. The LED is lightened by applying potential on the electrical contacts on the substrate.

Fig. 7(b)]. An assembled LED is aligned and bonded at the desired site after lubricant curing [see Fig. 7(c)].

In Fig. 8(a), we show an environmental scanning electron microscope (ESEM) image of an assembled LED. The gap between the LED and the substrate is approximately  $20 \mu\text{m}$ . Using the electroplating procedure described above, the gap is bridged by solder alloy [see Fig. 8(b)] and assembled LEDs can be activated by applying voltage to the electrical contacts on the substrate [see Fig. 3(b)]. Measured contact resistance is  $10 \Omega$  for the current design. An illustration of an activated glowing LED on a substrate is shown in Fig. 8(c).

As discussed above, both Au and Ni are demonstrated as good electroplating basis metals. However, there are several considerations that make Ni advantageous. When using Au bases, an extra desorption process is needed to remove the alkanethiol monolayer deposited on the bases. Also, we have observed severe wrinkling and peeling of SOG on Au after approximately two hours of desorption in the alkaline bath. This is due to poor adhesion between SOG and Au, particularly in alkaline solution (i.e., 0.5 M KOH) with potential bias applied to the Au areas. Tests of silicon nitride on Au during the desorption process have also shown wrinkling results. To overcome these problems Ni is chosen as an additional metal for electroplating basis. The Ni layer is also patterned as connections between the Au binding sites and the electrical contacts [see Fig. 3(b)] to reduce the contact area between Au and the passivation layer. With Ni beneath the passivation layer, it is observed that there are no signs of wrinkling after more than two hours, when performing SAM desorption.

## VI. SUMMARY AND FUTURE WORK

We have established a protocol based on capillary force and surface hydrophobicity modulation for multibatch micro self-assembly. Presented are the principles, fabrication, assembly, electroplating processes and pattern design of this technique. By incorporating a SAM desorption process into the self-assembly approach, multiple batch assembly becomes feasible. A two-batch micro assembly has been successfully demonstrated. The electroplating method is compatible with the parallel assembly process, and simultaneously achieves electrical connectivity for assembled components.

In our current experiments, an important parameter is the lubricant thickness. Preliminary simulation results in [35] show that critical behaviors of the parts are shift and twist displacement, and the restoration forces due to the shift and twist movements decrease with higher lubricant volume with given binding site size. Therefore, lubricant thickness control plays an important role in the assembly process. Studies of liquid microstructures in [14], [39] show liquid thickness increases with withdrawal speed from the interface. In addition the lubricant properties including surface tension, viscosity etc. can also be used to change the lubricant thickness. We plan to perform a study on the influences of these parameters on restoration forces, as well as on the alignment shift and twist precision.

Another important issue of the assembly is the scaling effect. In our experiments, assembly parts are in the millimeter scale. In [23], [28], parts are in the range of 150–400  $\mu\text{m}$  and in [20] parts are up to 5 mm in size. These self-assembly methods have been successful with part sizes ranging from hundreds of micrometers to several millimeters. With the lubricant thickness scaling with the binding site size [14], the driving force changes as well. It is anticipated that similar results can be obtained at smaller dimensions [40]. However, when approaching the nano scale, we might not use the long carbon chain lubricant to provide the driving force, as it might not form droplets of such small sizes. Therefore, understanding the scale effects of the driving force is of great importance for determining the optimal working domain for this technique.

In summary, as an enabling technique, our assembly approach is applicable to generic parts such as LEDs. It is anticipated that our controlled multi-batch self-assembly of micro devices technique can be applied to a wide range of micro or nano parts made of different materials, for the integration and packaging of complex heterogeneous systems.

## ACKNOWLEDGMENT

The authors would like to thank R. T. Howe and U. Srinivasan for inspiring discussions, and M. B. Cohn for providing some microparts, and S. Jiang and S. Chen for their help with the mica sample preparation. They also thank the members of the University of Washington MEMS lab and the staff and users of the Washington Technology Center Microfabrication laboratory for their help and support.

## REFERENCES

- [1] M. B. Cohn, "Assembly techniques for microelectromechanical systems," Ph.D. dissertation, Univ. California at Berkeley, Dep. Elect. Eng. Comput. Sci., 1997.
- [2] R. S. Fearing, "Survey of sticking effects for micro-parts," in *Proc. IEEE/RSJ Int. Conf. on Robotics and Intelligent Systems (IROS)*, Pittsburg, PA, 1995, pp. 212–217.
- [3] S. J. Ralis, B. Vikramaditya, and B. J. Nelson, "Micropositioning of a weakly calibrated microassembly system using coarse-to-fine visual servoing strategies," *IEEE Trans. Electronics. Packag. Manufact.*, vol. 23, pp. 123–131, 2000.
- [4] G. Yang, J. A. Gaines, and B. J. Nelson, "A flexible experimental work-cell for efficient and reliable wafer-level 3D micro-assembly," in *Proc. IEEE Int. Conference on Robotics and Automation (ICRA)*, Seoul, South Korea, 2001, pp. 133–138.
- [5] J. A. Thompson and R. S. Fearing, "Automating microassembly with ortho-tweezers and force sensing," in *Proc. IEEE/RSJ International Conference on Intelligent Robots and Systems (IROS)*, Maui, HI, 2001, pp. 1327–1334.
- [6] K. Saitou, D. A. Wang, and S. J. Wou, "Externally resonated linear microvibromotor for microassembly," *J. Microelectromech. Syst.*, vol. 9, pp. 336–346, Sept. 2000.
- [7] M. B. Cohn, K. F. Böhringer, J. M. Noworolski, A. Singh, C. G. Keller, K. Y. Goldberg, and R. T. Howe, "Microassembly technologies for MEMS," in *Proc. SPIE Micromachining and Microfabrication*, Santa Clara, CA, 1998, pp. 2–16.
- [8] A. S. Holmes and S. M. Saidam, "Sacrificial layer process with laser-driven release for batch assembly operations," *J. Microelectromech. Syst.*, vol. 7, no. 4, pp. 416–422, 1998.
- [9] G. M. Whitesides and B. Grzybowski, "Self-assembly at all scales," *Science*, vol. 295, pp. 2418–2421, 2002.
- [10] H. J. Yeh and J. S. Smith, "Fluidic assembly for the integration of GaAs light-emitting diodes on Si substrates," *IEEE Photon. Technol. Lett.*, vol. 46, pp. 706–709, 1994.
- [11] K. F. Böhringer, K. Y. Goldberg, M. B. Cohn, R. T. Howe, and A. P. Pisano, "Parallel microassembly using electrostatic force fields," in *IEEE Int. Conference on Robotics and Automation (ICRA)*, Leuven, Belgium, 1998, pp. 483–496.
- [12] J. Tien, A. Terfort, and G. M. Whitesides, "Microfabrication through electrostatic self-assembly," *Langmuir*, vol. 13, no. 20, pp. 5349–5355, 1997.
- [13] A. A. Darhuber, S. M. Troian, and S. Wagner, "Physical mechanisms governing pattern fidelity in microscale offset printing," *J. Appl. Phys.*, vol. 90, no. 7, pp. 3602–3609, 2001.
- [14] A. A. Darhuber, S. M. Troian, J. M. Davis, S. M. Miller, and S. Wagner, "Selective dip-coating of chemically micropatterned surfaces," *J. Appl. Phys.*, vol. 88, no. 9, pp. 5119–5126, 2000.
- [15] J. Lee and C. J. Kim, "Surface-tension-driven microactuation based on continuous electrowetting," *J. Microelectromech. Syst.*, vol. 9, no. 2, pp. 171–180, 2000.
- [16] K. F. Harsh, R. S. Irwin, and Y. C. Lee, "Solder self-assembly for MEMS," in *Proc. 1998 Int. Instrumentation Symposium (ISA)*, Reno, NV, 1998, pp. 256–261.

- [17] R. R. A. Syms, E. M. Yeatman, V. M. Bright, and G. M. Whitesides, "Surface tension self assembly of microstructures—the state of the art," *J. Microelectromech. Syst.*, to be published.
- [18] A. Terfort, N. Bowden, and G. M. Whitesides, "Three-dimensional self-assembly of millimeter-scale components," *Nature*, vol. 386, pp. 162–164, 1997.
- [19] A. Terfort and G. M. Whitesides, "Self-assembly of an operating electrical circuit based on shape complementarity and the hydrophobic effect," *Adv. Mater.*, vol. 10, no. 6, pp. 470–473, 1998.
- [20] D. Gracias, J. Tien, T. L. Breen, C. Hsu, and G. M. Whitesides, "Forming electrical networks in three dimensions by self-assembly," *Science*, vol. 289, pp. 1170–1172, 2000.
- [21] U. Srinivasan, R. T. Howe, and D. Liepmann, "Fluidic microassembly using patterned self-assembled monolayers and shape matching," in *Proc. 1999 Int. Conf. on Solid-State Sensors and Actuators (Transducers)*, Japan, 1999, pp. 1170–1173.
- [22] U. Srinivasan, D. Liepmann, and R. T. Howe, "Microstructure to substrate self-assembly using capillary Forces," *J. Microelectromech. Syst.*, vol. 10, no. 1, pp. 17–24, 2001.
- [23] H. O. Jacobs, A. R. Tao, A. Schwartz, D. H. Gracias, and G. M. Whitesides, "Fabrication of a cylindrical display by patterned assembly," *Science*, vol. 296, pp. 323–325, 2002.
- [24] M. N. Yousaf, B. T. Houseman, and M. Mrksich, "Using electroactive substrates to pattern the attachment of two different cell populations," in *Proc. National Academy of Sciences of the United States of America (PNAS)*, vol. 98, 2001, pp. 5992–5996.
- [25] M. D. Porter, T. B. Bright, D. L. Allara, and C. E. D. Chidsey, "Spontaneously organized molecular assemblies. 4. Structural characterization of n-alkyl thiol monolayers on gold by optical ellipsometry, infrared spectroscopy, and electrochemistry," *J. Amer. Chem. Soc.*, vol. 109, no. 12, pp. 3359–3568, 1987.
- [26] N. L. Abbot, A. B. Gorman, and G. M. Whitesides, "Active control of wetting using applied electrical potentials and self-assembled monolayers," *Langmuir*, vol. 11, no. 1, pp. 16–18, 1995.
- [27] M. M. Walczak, D. D. Popenoe, R. S. Deinhammer, B. D. Lamp, C. Chung, and M. D. Porter, "Reductive desorption of alkanethiolate monolayers at gold: a measure of surface coverage," *Langmuir*, vol. 7, no. 11, pp. 2687–2693, 1991.
- [28] U. Srinivasan, "Fluidic self-assembly of microfabricated parts to substrates using capillary forces," Ph.D. dissertation, Univ. California at Berkeley, Dep. Chem. Eng., 2001.
- [29] C. D. Bain, E. B. Troughton, Y. T. Tao, J. Ewall, G. M. Whitesides, and R. G. Nuzzo, "Formation of monolayer films by the spontaneous assembly of organic thiols from solution onto gold," *J. Amer. Chem. Soc.*, vol. 111, pp. 321–335, 1989.
- [30] S. Chen, L. Li, C. L. Boozer, and S. Jiang, "Controlled chemical and structural properties of mixed self-assembled monolayers of alkanethiols on Au(111)," *Langmuir*, vol. 16, no. 24, pp. 9287–9293, 2000.
- [31] A. J. Bard and L. R. Faulkner, *Electrochemical Methods: Fundamentals and Applications*, 1st ed. New York: Wiley, 1980.
- [32] J. A. Pojman, W. W. West, and J. Simmons, "Propagating fronts of polymerization in the physical chemistry laboratory," *J. Chem. Educ.*, vol. 74, no. 6, pp. 727–730, 1997.
- [33] K. F. Böhringer, U. Srinivasan, and R. T. Howe, "Modeling of capillary forces and binding sites for fluidic self-assembly," in *Proc. IEEE Workshop on Micro Electro Mechanical Systems (MEMS)*, Switzerland, 2001, pp. 369–374.
- [34] X. Xiong, Y. Hanein, W. Wang, D. T. Schwartz, and K. F. Böhringer, "Multi-batch micro-selfassembly via controlled capillary forces," in *Proc. IEEE/RSJ Int. Conference on Intelligent Robots and Systems (IROS)*, Maui, HI, 2001, pp. 1335–1342.
- [35] A. Greiner, J. Lienemann, J. G. Korvink, X. Xiong, Y. Hanein, and K. F. Böhringer, "Capillary forces in micro-fluidic self-assembly," in *Fifth Int. Conference on Modeling and Simulation of Microsystems (MSM'02)*, San Juan, Puerto Rico, Apr. 22–25, 2002.
- [36] K. Brakke, *Surface Evolver*. Selinsgrove, PA: Mathematics Department, Susquehanna University, 1999, pp. 1870–1001.
- [37] C. J. Zhong and M. D. Porter, "Fine structure in the voltammetric desorption curves of alkanethiolate monolayers chemisorbed at gold," *J. Electroanal. Chem.*, vol. 425, pp. 147–153, 1997.
- [38] J. W. Dini, *Electrodeposition: the Materials Science of Coatings and Substrates*, NJ: Noyes, 1993.
- [39] A. A. Darhuber, S. M. Troian, S. M. Miller, and S. Wagner, "Morphology of liquid microstructures on chemically patterned surfaces," *J. Appl. Phys.*, vol. 87, no. 11, pp. 7768–7775, 2000.

- [40] W. S. N. Trimmer, "Microrobots and micromechanical systems," *Sens. Actuators*, vol. 19, no. 3, pp. 267–287, 1989.



**Xiaorong Xiong** received the B.S. degree in mechanical engineering from Huazhong University of Science and Technology, China, and the M.S. degree in industrial engineering from University of Washington, Seattle. She is currently working toward the Ph.D. degree in electrical engineering at University of Washington.

In 2001–2002, she was the recipient of a Ford Fellowship. Her research includes development of micro-assembly technique for microsystem integration.



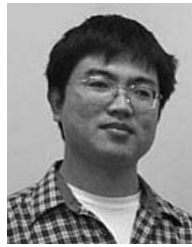
**Yael Hanein** (M'00) received the B.Sc. degree in physics from Tel-Aviv University, Israel, and the M.Sc. and Ph.D. degrees in physics from the Weizmann Institute of Science, Israel.

She is currently a Research Associate in the Physics Department at University of Washington, Seattle, and a Visiting Scientist at the Tel-Aviv nanotechnology center. Her current interests include BioMEMS, micro-self-assembly, and carbon nanotube electronic devices.



**Jiandong Fang** received the B.S. degree in physics from University of Science and Technology, China, in July of 1999 and the M.S. degree in physics from University of Washington, Seattle, in March of 2001. Currently, he is pursuing the Ph.D. degree in electrical engineering at University of Washington.

His research includes fluidic self-assembly of microcomponents, development of micropump devices.



**Yanbing Wang** received the B.S. degree in physics from Peking University, China, in 1997 and the M.S. degree in physics from University of Washington, Seattle, in 2001. He is currently pursuing the Ph.D. degree in electrical engineering at the University of Washington.

His research includes the development of programmable surface chemistry with ppNIPAM and its application in MEMS self-assembly and bioMEMS.



**Weihua Wang** received the B.S. degree in chemical engineering from Zhejiang University, China, and the Ph.D. degree from the University of Washington, Seattle, in 2002.

She is currently employed at ATMI, Danbury, CT.

Dr. Wang was the recipient of numerous awards while a Ph.D. student, including an Abner Brenner Student Travel Grant from the Electrochemical Society in 1999, a Surface Finishing Scholarship from the American Electroplaters and Surface Finishers Society in 2001, and was coauthor of the

prize winning student poster at the 2001 joint meeting of ISE and ECS.



**Daniel T. Schwartz** received the B.S. degree in chemical engineering from University of Minnesota, Minneapolis, in 1983 and the M.S. and Ph.D. degrees from the University of California at Davis in 1985 and 1989, respectively.

In 1991, he completed a Postdoctoral Fellowship at the Materials Science Division of Lawrence Berkeley National Laboratory, and joined the faculty of the University of Washington, Seattle. He is currently Professor of Chemical Engineering and Director of the Electrochemical Materials and Inter-

faces Laboratory (EMIL). EMIL research tackles processing-structure-property relationships in materials and interfaces synthesized electrochemically.

Prof. Schwartz has taken an active role in the electrochemical materials community, having served as Chairman for the 2002 Gordon Research Conference on Electrodeposition, and as Chairman (2001–2003) of the Electrochemical Society's Electrodeposition Division.



**Karl F. Böhringer** (S'94–M'97) received the M.S. and Ph.D. degrees in computer science from Cornell University, Ithaca, NY, and the Diplom-Informatiker degree from the University of Karlsruhe, Germany.

He is currently an Assistant Professor in Electrical Engineering with adjunct appointments in Computer Science & Engineering and in Mechanical Engineering at the University of Washington, Seattle. During his dissertation work on distributed micro-manipulation he designed, built, and tested multiple microactuator arrays at the Cornell Nanofabrication

Facility. He also spent a year as a Visiting Scholar at the Stanford Robotics Lab and Transducer Lab, where he collaborated on research in MEMS cilia arrays. From 1996 to 1998, he investigated techniques for parallel micro-self-assembly as a Postdoctoral Researcher at the University of California, Berkeley. His current interests include micromanipulation and microassembly, as well as biomedical implants and bioMEMS for single-cell genomics and proteomics. At the University of Washington, he is a member of the Center for Nanotechnology and the NIH Microscale Life Sciences Center.

Dr. Böhringer was nominated for the ACM doctoral dissertation award for his Ph.D. dissertation. He received an NSF Postdoctoral Associateship in 1997, an NSF CAREER award in 1999, and was an NSF New Century Scholar in 2000. His work is featured in the Top 100 Science Stories in *Discover* magazine's 2002 "Year in Science".

## Errata

“Controlled Multibatch Self-Assembly of Microdevices,” by Xiaorong Xiong, Yael Hanein, Jiandong Fang, Yanbing Wang, Weihua Wang, Daniel T. Schwartz, and Karl F. Böhringer, *ASME/IEEE Journal of Microelectromechanical Systems*, vol. 12, no. 2, pp. 117-127, April 2003.

In Figure 5, p. 123, the axis labels are missing. The horizontal axis should be labeled  $V$ , and the vertical axes should all be labeled  $\mathbf{mA/cm}^2$ .